Transfer Learning for Image-Based Malware Classification

Niket Bhodia[1], Pratikkumar Prajapati[1], Fabio Di Troia[1] and Mark Stamp[1]
[1]*Department of Computer Science, San Jose State University, San Jose, California, USA*
niket.bhodia@sjsu.edu, pratikkumar.prajapati@sjsu.edu, fabioditroia@msn.com, mark.stamp@sjsu.edu

Keywords: Malware; machine learning; deep learning; transfer learning; *k*-nearest neighbor.

Abstract: In this paper, we consider the problem of malware detection and classification based on image analysis. We convert executable files to images and apply image recognition using deep learning (DL) models. To train these models, we employ transfer learning based on existing DL models that have been pre-trained on massive image datasets. We carry out various experiments with this technique and compare its performance to that of an extremely simple machine learning technique, namely, *k*-nearest neighbors (*k*-NN). For our *k*-NN experiments, we use features extracted directly from executables, rather than image analysis. While our image-based DL technique performs well in the experiments, surprisingly, it is outperformed by *k*-NN. We show that DL models are better able to generalize the data, in the sense that they outperform *k*-NN in simulated zero-day experiments.

1 INTRODUCTION

Traditionally, malware detection has relied on pattern matching against signatures extracted from known malware. While simple and efficient, signature scanning is easily defeated by a number of well-known evasive strategies. This fact has given rise to statistical and machine learning based detection techniques, which are more robust to code modification. In response, malware writers have developed advanced forms of malware that alter statistical and structural properties of their code. Such "noise" can cause statistical models to misclassify samples.

In this paper, we compare image-based deep learning (DL) models for malware analysis to a much simpler non-image based technique. To train these DL models, we employ transfer learning, relying on models that have been pre-trained on large image datasets. Leveraging the power of such models has been shown to yield strong malware detection and classification results (Yajamanam et al., 2018). Intuitively, we might expect that models based on image analysis to be more robust, as compared to models that rely on opcodes, byte *n*-grams, or similar statistical features (Damodaran et al., 2017), (Singh et al., 2016), (Toderici and Stamp, 2013), (Baysa et al., 2013), (Austin et al., 2013), (Wong and Stamp, 2006).

To the best of our knowledge, image analysis was first applied to the malware problem in (Nataraj et al., 2011), where high-level "gist" descriptors were used. More recently, (Yajamanam et al., 2018) confirmed these results and contrasted the gist-descriptor method to a DL approach that produced equally good—if not slightly better—results without the extra work required to extract gist descriptors. A direct comparison to more straightforward machine learning techniques seems to be lacking in previous work, making it difficult to determine the comparative advantages and disadvantages of DL image-based analysis in the malware domain.

In this paper, we extend the analysis found in (Yajamanam et al., 2018) in various directions. For example, we consider improvements to the DL training, and we apply our improved image-based DL approach to a more challenging dataset. Most significantly, we compare the performance of image-based DL analysis to a relatively simple and straightforward non-image based strategy using *k*-nearest neighbors (*k*-NN). These *k*-NN experiments yield somewhat surprising results and serve to highlight the strengths and weaknesses of DL image-based analysis.

2 METHODOLOGY

In this section, we discuss the datasets, data preprocessing, and features extracted. We also discuss implementation details.

2.1 Datasets

We consider two malware datasets, namely, Malimg (Nataraj et al., 2011) and Malicia (Nappa et al., 2015). The Malimg dataset contains 9,339 malware images from 25 families, while Malicia has 11,668 malware binaries from 54 families.

The Malimg dataset consists of images, and hence these samples require no pre-processing before applying image-based analysis. However, the binaries corresponding to the Malimg images are not readily available. In contrast, the Malicia samples are binaries and hence they must be converted into images before we can apply image-based analysis. We found that 581 samples from the Malicia dataset were not `exe` files, and 1,192 samples did not have a family label. These samples were excluded, leaving us with 9,895 binaries from 51 families from the Malicia dataset.

The family breakdown for the Malimg and Malicia datasets are given in Tables 1 and 2, respectively. In Table 1, we abbreviate “password stealing” as “pws,” “downloader” as “dl,” and “backdoor” as “bd.” In Table 2, the “other” category consists of 38 families, each of which has less than 10 samples per family, with the majority of these “families” contributing only a single sample.

In addition, two benign datasets were used. The first of these benign sets consists of 3304 binaries typically found on a modern Windows PC. Our second benign dataset contains 704 binaries from the Cygwin library.

2.2 Data Preprocessing

Our DL method requires images as input. For Malimg, we directly use the images that comprise the dataset—the only preprocessing involves separating the images into training and validation sets. For Malicia, we have malware binaries, which are converted to images by adapting the script used by the authors of (Nataraj et al., 2011). More details on this image conversion process are provided in Section 2.3.

从二进制文件中提取特征信息作为KNN的输入

For our *k*-NN experiments, we do not use images, but instead extract a set of features directly from binaries. More details on these features are provided in Section 2.4. Since we did not have access to Malimg binaries, we could not test our *k*-NN approach on this dataset. We compare our *k*-NN results to image-based DL using the the Malicia samples.

The Malicia dataset is highly unbalanced—four families dominate, as can be seen from the counts in Table 2. Hence, we have partitioned the dataset into two parts, with one set containing only samples from the large families and one containing all samples from the small families, where we consider any family with more than 100 samples to be “large.” Both of these Malicia subsets are used in different variations of our experiments.

Table 1: Malimg dataset

Family	Type	Samples
Adialer.C	dialer	122
Agent.FYI	bd	116
Allaple.A	worm	2,949
Allaple.L	worm	1,591
Alueron.gen!J	trojan	198
Autorun.K	worm	106
C2LOP.gen!g	trojan	200
C2LOP.P	trojan	146
Dialplatform.B	dialer	177
Dontovo.A	dl	162
Fakerean	rogue	381
Instantaccess	dialer	431
Lolyda.AA1	pws	213
Lolyda.AA2	pws	184
Lolyda.AA3	pws	123
Lolyda.AT	pws	159
Malex.gen!J	trojan	136
Obfuscator.AD	dl	142
Rbot!gen	bd	158
Skintrim.N	trojan	80
Swizzor.gen!E	dl	128
Swizzor.gen!I	dl	132
VB.AT	worm	408
Wintrim.BX	dl	97
Yuner.A	worm	800
Total	—	9,339

Python科学数据手册

科学手册.

类似的

丝毫

丝毫没有

Table 2: Malicia dataset

Family	Samples	Size
cleaman	32	small
CLUSTER:46.105.131.121	20	small
CLUSTER:85.93.17.123	45	small
CLUSTER:astaror	24	small
CLUSTER:newavr	29	small
CLUSTER:positivtkn.in.ua	14	small
cridex	74	small
harebot	53	small
securityshield	150	large
smarthdd	68	small
winwebsec	5,820	large
zbot	2,167	large
zeroaccess	1,306	large
other (38 families)	93	small
Total	9,895	—

2.3 Converting Binaries to Images

宽度256
长度变

To convert a binary to an image we treat the sequence of bytes representing the binary as the bytes of a grayscale PNG image. In all of our experiments, we use a predefined width of 256, and a variable length, depending on the size of the binary.

Sample images of unrelated binaries are given in Figure 1, while samples from a malware family appear in Figure 2. From these examples, the allure of image-based classification is clear—images tend to smooth out minor within-family differences, while significant (i.e., between family) differences are clearly observed.

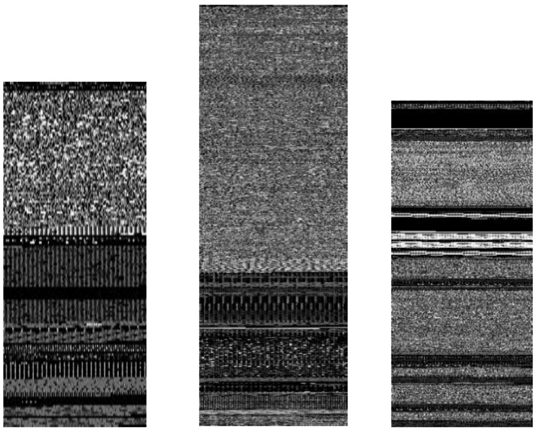

Figure 1: Unrelated binaries as images

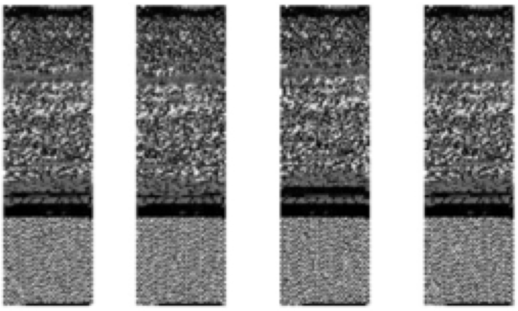

Figure 2: Variants of malware from the Malimg family of Dialplatform.B as images (Nappa et al., 2015)

2.4 Feature Extraction for k-NN

We adapted code from two publicly accessible GitHub repositories (PE File, 2018) and (Machine Learning, 2018) to extract 54 features from each binary sample. For the sake of brevity, we list 15 of these 54 features in Table 3, where feature names are listed in the left-hand column, while the right-hand column gives the feature value extracted from the benign sample VC_redist.x64.

Table 3: Examples of k-NN features

Name	VC_redist.x64
SizeOfOptionalHeader	224
SizeOfCode	234496
FileAlignment	512
MajorOSVersion	5
SizeOfImage	413696
SizeOfHeaders	1024
Subsystem	2
SizeOfStackCommit	4096
SectionsNb	7
SectionsMeanEntropy	3.7137
SectionMaxRawsize	234496
SectionMaxVirtualsize	234372
ImportsNb	285
ResourcesMaxEntropy	5.2550
ResourcesMaxSize	9652

2.5 Implementation Details

The DL models were implemented using the fast.ai library (Fast.ai, 2018), which is built on top of the PyTorch framework. The choice of this library was influenced by the fact that it incorporates several DL best practices, including learning rate finding, stochastic gradient descent with restarts, and differential learning rates.

For k-NN, we used the popular Scikit-learn library (Pedregosa et al., 2011), which is based on many of the fundamentals described in (Stamp, 2017). The fast.ai library incorporates CUDA support, which allowed us to accelerate the training process by making use of the graphics card.

3 EXPERIMENTS AND RESULTS

We performed a variety of experiments involving various combinations of datasets, classification level (binary and multiclass), and learning techniques (DL and k-NN). Here, we present results for eight separate experiments, as listed in Table 4. Each experiment represented a specific combination of datasets, classification level, and learning technique. In the remainder of this section, we discuss each of these experiments in some detail.

For the DL experiments, that is, experiments 1 through 4 in Table 4, we tested variants of the ResNet model (He et al., 2016), specifically, ResNet34, ResNet50, ResNet101, and ResNext50. We chose ResNet because of its combination of performance

Table 4: Experiments

Number	Classification	Malware dataset	Benign dataset	Learning technique	Accuracy
1	binary	Malimg	Windows	DL	98.39%
2	multiclass (26)	Malimg	Windows	DL	94.80%
3	binary	Malicia (large)	Windows	DL	97.61%
4	multiclass (5)	Malicia (large)	Windows	DL	92.93%
5	binary	Malicia (large)	Windows	k-NN	99.60%
6	multiclass (5)	Malicia (large)	Windows	k-NN	99.43%
7	binary (zero-day)	Malicia (small)	Cygwin	DL	91.17%
8	binary (zero-day)	Malicia (small)	Cygwin	k-NN	89.00%

and efficiency. ResNet-based architectures won the ImageNet and COCO challenges in 2015. Their key advantage is the use of "residual blocks," which enabled the training of neural networks of unprecedented depth. The models we use were pre-trained on the ImageNet dataset, which contains some 1.2 million images in 1,000 classes.

The more complex ResNet variants we experimented with did not yield significant improvement, so we used ResNet34 for all DL experiments reported in this paper. We also tested various combinations of hyperparameters, including the number of epochs, the learning rate, the number of cycles of learning rate annealing, and variations in the cycle length. The training concepts implemented in conjunction with these hyperparameters were cosine annealing, learning rate finding, stochastic gradient descent with restarts, freezing and unfreezing layers in the pre-trained network, and differential learning rates. A description of these techniques and how they are used in concert with the listed hyperparameters is beyond the scope of this paper—the interested reader can refer to (Yajamanam et al., 2018), (Fast.ai, 2018), and (Smith, 2015) for more details.

余弦退火

带重启的随机梯度下降.

lr衰减至较小值后恢复到初始值

Perhaps the simplest machine learning technique possible is k-NN, where we classify a sample based on its k nearest neighbors in a given training set. For k-NN, there is no explicit training phase, and all work is deferred to the scoring phase. Once the training data is specified, we score a sample by simply determining its nearest neighbors in the training set, with a majority vote typically used for (binary) classification. In spite of its incredible simplicity, it is often the case that k-NN achieves results that are competitive with far more complex machine learning techniques (Stamp, 2017).

For our k-NN experiments (i.e., experiments 5 and 6), we use Euclidean distance, and hence the only parameter to be determined is the value of k, that is, the number of neighbors to consider when classifying a sample. We experimented with values ranging from $k = 1$ to $k = 9$, and we found that the best results were obtained with $k = 1$, as can be seen in both Figures 8(a) and 9(a). Thus, we have used $k = 1$ for the k-NN results presented in this paper. Again, for these experiments, the feature vector consists of 54 PE file features extracted using modified forms of the code at (PE File, 2018) and (Machine Learning, 2018).

4 DISCUSSION

For our first set of experiments, we apply the image-based DL technique outlined above to the Malimg dataset. We consider the following two variations.

Experiment 1 For our first experiment, we perform binary classification of malware versus benign, where the malware class is obtained by simply grouping all Malimg families into one malware set. The benign set consists of 3304 Windows samples, which have been converted to images.

Experiment 2 For the corresponding multiclass classification problem, we attempt to classify the malware samples into their respective families, with the Windows benign set treated as an additional "family." Since there are 25 malware families in the Malimg dataset, for this classification problem, we have 26 classes.

For the binary classification problem in experiment 1, we obtained an accuracy of 98.39%, while the multiclass problem in experiment 2 yielded an accuracy of 94.80%. The results of experiment 1 are summarized in Figure 3, while Figures 4 and 5 give the results for experiment 2. These experimental results are comparable to those obtained in (Yajamanam et al., 2018), and serve to confirm our DL implementation.

We do not have access to the Malimg binary files, so we are unable to compare the DL results for this dataset to alternatives that rely on features extracted

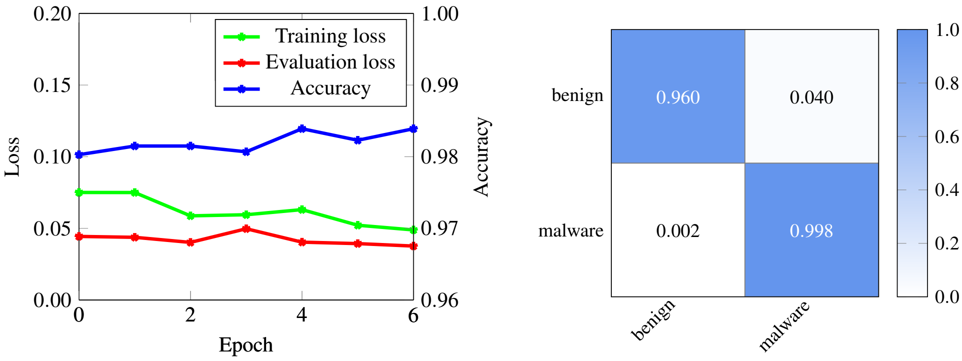

(a) Training (b) Confusion matrix

Figure 3: Experiment 1 results

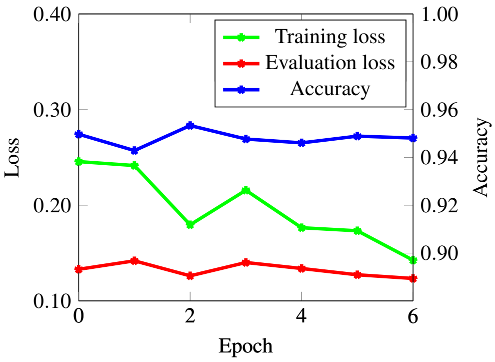

Figure 4: Experiment 2 training

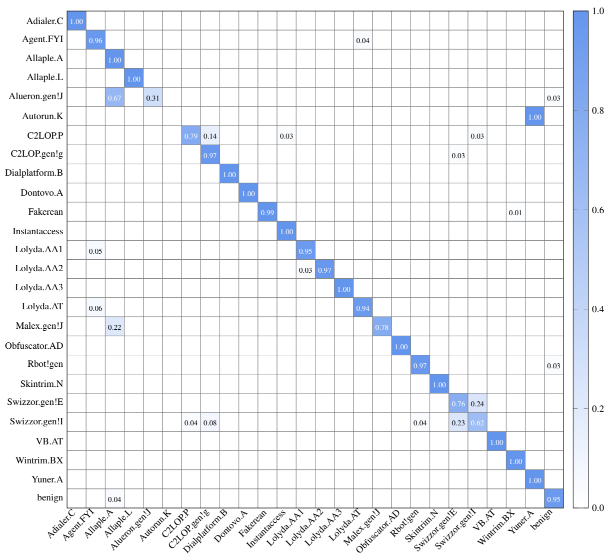

Figure 5: Experiment 2 confusion matrix

directly from executables. Therefore, we next consider the Malicia malware dataset, which will allow us to compare our image-based DL technique to a simpler *k*-NN analysis based on non-image features.

For the Malicia dataset, we first generate an image corresponding to each binary executable sample in the dataset, as discussed in Section 2.3. Then we perform the analogous experiments to 1 and 2, above, but using the Malicia samples in place of Malimg. Specifically, we perform the following experiments.

Experiment 3 As in experiment 1, we perform binary classification of malware versus benign, but in this case, the malware class consists of all Malicia samples, as images. The benign set consists of the same 3304 Windows samples that were used in experiment 1.

Experiment 4 For the corresponding multiclass version of this problem, we attempt to classify the Malicia (image) samples into their respective families, with the Windows benign set treated as an additional "family."

For the binary classification problem in experiment 3, we obtain an accuracy of 97.61%, while the multiclass problem in experiment 4 yields a classification accuracy of 92.93%. The results of experiment 3 are summarized in Figure 6, while Figure 7 contains the results of experiment 4. Note that only the four large Malicia families were used in these experiments, as the remaining families are severely underrepresented in the dataset. These results indicate that the multiclass problem is far more challenging for the Malicia dataset, as compared to the Malimg dataset. Recall that there are 26 classes in the Malimg classification experiment, but only five classes in the corresponding Malicia experiment, yet we obtain a lower multiclass accuracy on the Malicia samples.

Next, we compare our DL approach to a simpler strategy based on *k*-NN. We extract non-image features from the Malicia binaries and the benign set, as discussed in Section 2.4. Then we carry out binary

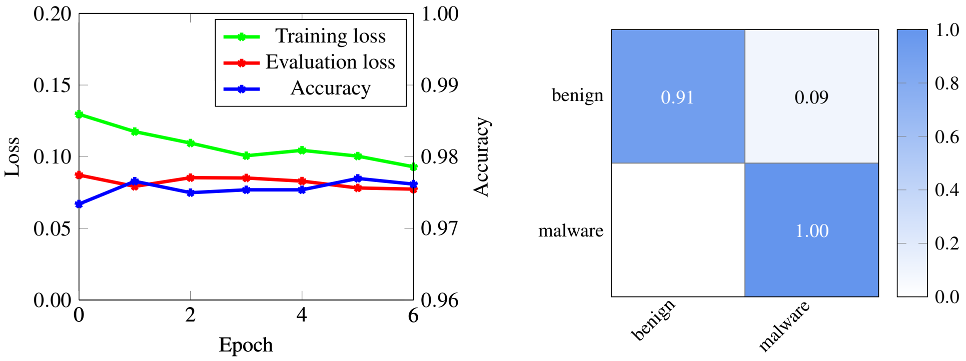

(a) Training (b) Confusion matrix

Figure 6: Experiment 3

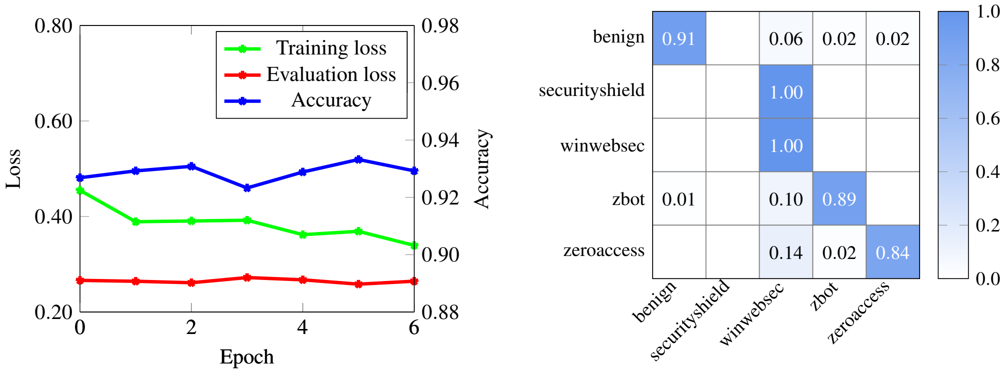

(a) Training (b) Confusion matrix

Figure 7: Experiment 4

and multiclass experiments. Specifically, we perform the following k-NN experiments.

Experiment 5 For this binary classification experiment, we deal with malware and benign sets, where the malware class consists of Malicia samples. In this case, non-image features are extracted directly from the malware binaries. The benign set again consists of the 3304 Windows samples, and the same non-image features have been extracted from these samples.

Experiment 6 In the corresponding multiclass experiment, we attempt to categorize the Malicia samples into their respective families, with the Windows benign set treated as a yet another "family." As above, here we only use the four large Malicia families which, together with the benign set, gives us a total of five distinct classes.

As mentioned above, we selected k-NN for these experiments because we want to establish a baseline by which to compare the performance of our image-based DL approach. We also want to use non-image features in this alternative analysis, as this provides some additional insight into the value of treating malware samples as images.

Interestingly, k-NN outperforms DL, achieving an impressively high accuracy of 99.60% in the binary classification problem, while a similarly high accuracy of 99.43% is attained in the multiclass problem. Figures 8 and 9, respectively, summarize the results of experiment 5 and experiment 6. Note that the multiclass result in experiment 6 is particularly strong, given that there are five classes under consideration, including a benign set. In contrast, our image-based DL technique yielded substantially worse results, with an accuracy of less than 93% on this same dataset.

Next, we attempt to quantify the robustness and generalizability of our DL (image-based) technique in comparison to our k-NN (`exe`-based) classification strategy. For the DL and k-NN cases, denoted here as experiments 7 and 8, respectively, we attempt to classify samples as malware or benign, based on sam-

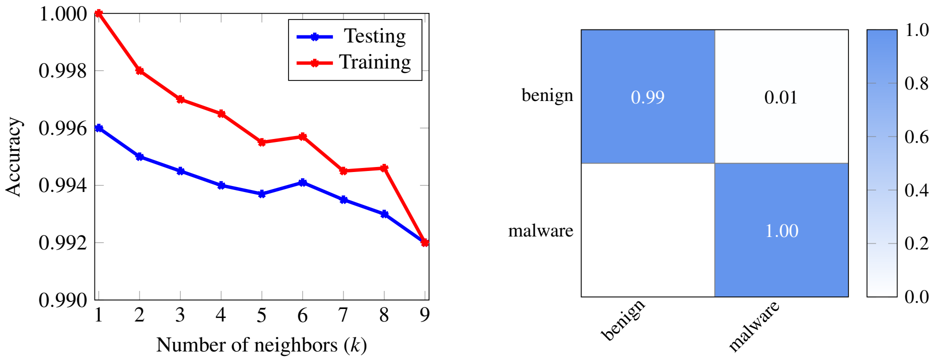

(a) Determining optimal k (b) Confusion matrix

Figure 8: Experiment 5

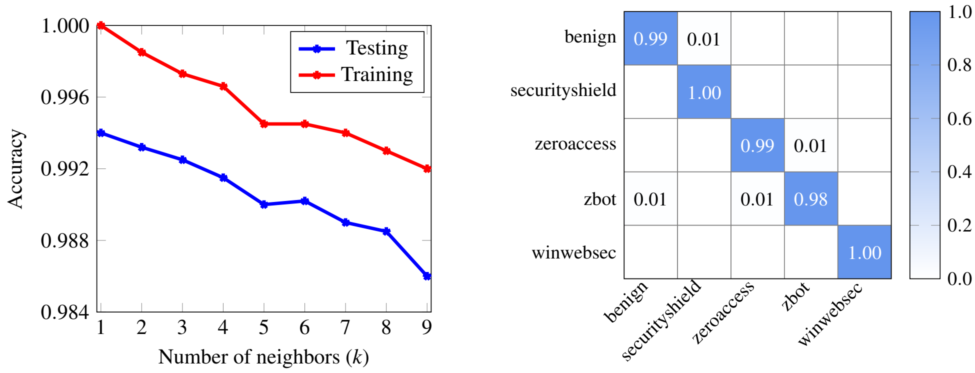

(a) Determining optimal k (b) Confusion matrix

Figure 9: Experiment 6

zero-day:
测试样本属于的家族不在训练集中．即在不训练对应family的情况测试该家族的样本

ples belonging to families that the models have not been trained to detect. This can be viewed as simulating zero-day malware, that is, malware that was not available during the training phase. Specifically, we performed the following zero-day experiments.

Experiment 7 We test our DL approach for the binary classification of zero-day malware versus benign, where the malware training set consists of all samples in the four large Malicia families. The benign training set consists of 3304 Windows samples. To simulate zero-day malware, the test set consists of all of the small families in the Malicia dataset. In addition, to ensure that unfamiliar benign binaries did not lead to a high false positive rate, we used 704 Cygwin binaries as our benign test set.

大家族作为训练集中．小家族作为测试集 因此为zero-day.

Experiment 8 For our corresponding k-NN experiments, we use the same datasets as in experiment 7. And, as above, to simulate zero-day malware, the malware test set consists of all of the small families in the Malicia dataset, and the benign test set consists of the 704 Cygwin samples.

测试集中良性样本也是训练集中没有的Cygwin.

Our image-based DL model performed reasonably well in this zero-day simulation, correctly identifying 79% of the malware samples, with a low false positive rate of 1%. However, our DL model has a high false negative rate, as illustrated in Figure 10 (a). With k-NN, we achieve broadly similar, but somewhat worse results, as can be seen from the confusion matrix in Figure 10. These zero-day experiments indicate that image-based DL models generalize somewhat better than a more straightforward k-NN model. This is a potentially an advantage for image-based DL models in the malware realm, as detecting zero-day malware is the holy grail in the AV field. However, the simplicity and ease of training k-NN models could be a major advantage in some situations.

→假阴性率较高．即将正常样本误报为恶意样本

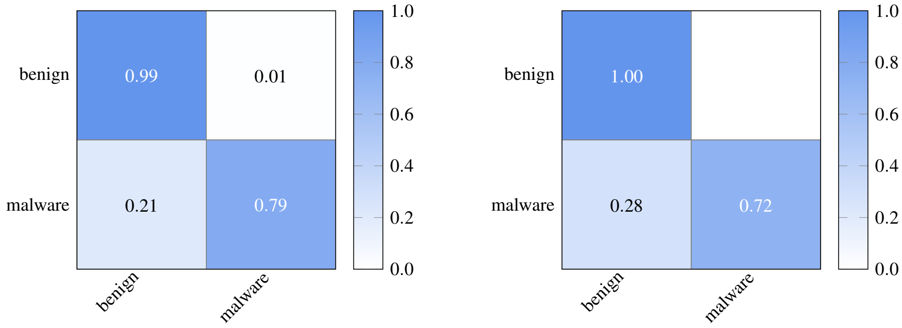

(a) DL results

(b) k-NN results

Figure 10: Zero-day simulations (experiments 7 and 8)

5 CONCLUSION

In this paper, we treated malware binaries as images and classified samples based on pre-trained deep learning image recognition models. We compared these image-based deep learning (DL) results to a simpler k-nearest neighbor (k-NN) approach based on a more typical set of static features. We carried out a wide variety of experiments, each representing a different combination of dataset, classification level, and learning technique. The multiclass experiments were particularly impressive, with high accuracy attained over a large number of malware families.

Our DL method overall delivered results comparable to previous work, yet it was outperformed by the much simpler k-NN learning technique in some cases. The image-based DL models did outperform k-NN in simulated zero-day experiments, which indicates that this DL implementation better generalizes the training data, as compared to k-NN. This is a significant point, since zero-day malware, arguably, represents the ultimate challenge in malware detection.

There are many promising avenues for future work related to image-based malware analysis. For example, it seems likely that a major strength of any image-based strategy is its robustness. Consequently, additional experiments along these lines would be helpful to better quantify this effect.

REFERENCES

Austin, T. H., Filiol, E., Josse, S., and Stamp, M. (2013). Exploring hidden Markov models for virus analysis: A semantic approach. In *46th Hawaii International Conference on System Sciences, HICSS 2013, Wailea, HI, USA, January 7-10, 2013*, pages 5039–5048. IEEE Computer Society.

Baysa, D., Low, R. M., and Stamp, M. (2013). Structural entropy and metamorphic malware. *Journal of Computer Virology and Hacking Techniques*, 9(4):179–192.

Damodaran, A., Troia, F. D., Visaggio, C. A., Austin, T. H., and Stamp, M. (2017). A comparison of static, dynamic, and hybrid analysis for malware detection. *Journal of Computer Virology and Hacking Techniques*, 13(1):1–12.

Fast.ai (2018). Fast.ai lectures. https://course.fast.ai/lessons/lessons.html.

He, K., Zhang, X., Ren, S., and Sun, J. (2016). Deep residual learning for image recognition. In *2016 IEEE Conference on Computer Vision and Pattern Recognition*, CVPR 2016, pages 770–778.

Machine Learning (2018). Machine learning: Github repository. https://github.com/tuff96/Malware-detection-using-Machine-Learning.

Nappa, A., Rafique, M. Z., and Caballero, J. (2015). The Malicia dataset: Identification and analysis of drive-by download operations. *International Journal of Information Security*, 14(1):15–33.

Nataraj, L., Karthikeyan, S., Jacob, G., and Manjunath, B. (2011). Malware images: Visualization and automatic classification. In *Proceedings of the 8th International Symposium on Visualization for Cyber Security*, VizSec '11.

PE File (2018). Pe file: Github repository. https://github.com/erocarrera/pefile.

Pedregosa, F., Varoquaux, G., Gramfort, A., Michel, V., Thirion, B., Grisel, O., Blondel, M., Prettenhofer, P., Weiss, R., Dubourg, V., Vanderplas, J., Passos, A., Cournapeau, D., Brucher, M., Perrot, M., and Duchesnay, E. (2011). Scikit-learn: Machine learning in python. *J. Mach. Learn. Res.*, 12:2825–2830.

Singh, T., Troia, F. D., Visaggio, C. A., Austin, T. H., and Stamp, M. (2016). Support vector machines and malware detection. *Journal of Computer Virology and Hacking Techniques*, 12(4):203–212.

Smith, L. N. (2015). Cyclical learning rates for training neural networks. https://arxiv.org/abs/1506.01186.

Stamp, M. (2017). *Introduction to Machine Learning with Applications in Information Security*. Chapman and Hall/CRC, Boca Raton.

Toderici, A. H. and Stamp, M. (2013). Chi-squared distance and metamorphic virus detection. *Journal of Computer Virology and Hacking Techniques*, 9(1):1–14.

Wong, W. and Stamp, M. (2006). Hunting for metamorphic engines. *Journal in Computer Virology*, 2(3):211–229.

Yajamanam, S., Selvin, V. R. S., Troia, F. D., and Stamp, M. (2018). Deep learning versus gist descriptors for image-based malware classification. In *Proceedings of the 4th International Conference on Information Systems Security and Privacy*, ICISSP 2018, pages 553–561.